# Accepted Manuscript


Novel $Ba(Gd_{1-x}Y_x)_{0.78}F_5$: 20 mol% $Yb^{3+}$, 2 mol% $Tm^{3+}$ ($0 \leq x \leq 1.0$) solid solution nanocrystals: A facile hydrothermal controlled synthesis, enhanced upconversion luminescent and paramagnetic properties

Tao Li, Yanmei Li, Ran Luo, Zhanglei Ning, Yan Zhao, Mengjiao Liu, Xin Lai, Cheng Zhong, Chao Wang, Jingquan Zhang, Jian Bi, Daojiang Gao

PII: S0925-8388(18)30041-0

DOI: 10.1016/j.jallcom.2018.01.040

Reference: JALCOM 44504

To appear in: *Journal of Alloys and Compounds*

Received Date: 24 October 2017

Revised Date: 2 January 2018

Accepted Date: 3 January 2018

Please cite this article as: T. Li, Y. Li, R. Luo, Z. Ning, Y. Zhao, M. Liu, X. Lai, C. Zhong, C. Wang, J. Zhang, J. Bi, D. Gao, Novel $Ba(Gd_{1-x}Y_x)_{0.78}F_5$: 20 mol% $Yb^{3+}$, 2 mol% $Tm^{3+}$ ($0 \leq x \leq 1.0$) solid solution nanocrystals: A facile hydrothermal controlled synthesis, enhanced upconversion luminescent and paramagnetic properties, *Journal of Alloys and Compounds* (2018), doi: 10.1016/j.jallcom.2018.01.040.

# Novel $Ba(Gd_{1-x}Y_x)_{0.78}F_5$: 20 mol% $Yb^{3+}$, 2 mol% $Tm^{3+}$ ($0 \leq x \leq 1.0$) solid solution nanocrystals: a facile hydrothermal controlled synthesis, enhanced upconversion luminescent and paramagnetic properties

Tao Li[a], Yanmei Li[a], Ran Luo[a], Zhanglei Ning[a], Yan Zhao[a], Mengjiao Liu[a], Xin Lai [a*], Cheng Zhong[b], Chao Wang[c], Jingquan Zhang[d], Jian Bi[a], Daojiang Gao[a*]

[a] *College of Chemistry and Materials Science, Sichuan Normal University, Chengdu 610068, China*

[b] *Department of Basic Education, Dazhou Vocational and Technical College, Dazhou 635001, China*

[c] *Clean Energy Materials and Engineering Center, School of Microelectronics and Solid-state Electronics, University of Electric Science and Technology of China, Chengdu 611731, China*

[d] *Institute of Solar Energy Materials and Devices, College of Materials Science and Engineering, Sichuan University, Chengdu 610064, China*

Corresponding author: Xin Lai and Daojiang Gao

E-mail address: laixin1972@126.com; daojianggao@sicnu.edu.cn;

daojianggao@126.com

**Abstract:** $Ba(Gd_{1-x}Y_x)_{0.78}F_5$: 20 mol% $Yb^{3+}$, 2 mol% $Tm^{3+}$ ($0 \leq x \leq 1.0$) solid solution nanocrystals were successfully synthesized via a facile hydrothermal method, the obtained crystals were characterized by X-ray diffraction (XRD), scanning electron microscopy (SEM), the transmission electron microcopy (TEM), energy dispersion spectrometry (EDS), photoluminescence (PL) as well as vibrating sample magnetometer (VSM), respectively. The influences of the concentration of yttrium ion ($Y^{3+}$) on the microstructures, upconversion (UC) luminescent and magnetic properties of the $Ba(Gd_{1-x}Y_x)_{0.78}F_5$: 20 mol% $Yb^{3+}$, 2 mol% $Tm^{3+}$ samples have been deeply investigated. XRD results showed that all the $Ba(Gd_{1-x}Y_x)_{0.78}F_5$: 20 mol% $Yb^{3+}$, 2 mol% $Tm^{3+}$ crystals are continuous solid solution possess a pure cubic phase structure. SEM and TEM results revealed that all the obtained crystals are quasi-spherical nanocrystals with a diameter ranging from ~55 nm to ~240 nm, and the doping of $Y^{3+}$ ion can inhibit the grain growth. PL spectra indicated that all the samples exhibit main blue emission centered at 478 nm ascribed to $^1G_4 \rightarrow {}^3H_6$ transition of $Tm^{3+}$ ions, and its UC emission intensity initially increases and then notably decreases with increasing content of $Y^{3+}$ ion, giving the maximum at x=0.8. VSM results showed that all the samples present benign paramagnetism in the magnetic range of -30 to 30 kOe at 300 K due to no coercivity or no remanence. Our results confirm that the UC luminescence properties of the $Ba(Gd_{1-x}Y_x)_{0.78}F_5$: 20 mol% $Yb^{3+}$, 2 mol% $Tm^{3+}$ nanocrystals can be effectively modulated through the replacement of $Gd^{3+}$ ions by $Y^{3+}$ ions, which also can provide a relatively clear understanding of the formation process and the enhancement mechanism

of UC emission for other rare earth polyfluoride solid solution nanocrystals.

**Keywords**: $Ba(Gd_{1-x}Y_x)_{0.78}F_5$: 20 mol% $Yb^{3+}$, 2 mol% $Tm^{3+}$ solid solution; nanocrystals; hydrothermal synthesis; UC luminescent properties; paramagnetic properties

## 1. Introduction

In recent years, rare earth fluoride luminescent materials have attracted much attention due to their outstanding thermal stability, chemical durability, and unique optical properties including low phonon energy (<400 $cm^{-1}$), high refractive index, wide color range as well as high energy transfer efficiency [1-6]. Nowadays, fluorides doped with lanthanide ions have been widely used in the fields such as lighting [7-8], three-dimensional display [9-11] and biological labeling [12-15], thus leading the rare earth doped fluoride to be a kind of useful and indispensable multifunctional material.

Among the various rare earth fluorides, alkali metal rare earth fluorides and alkaline-earth metal rare earth fluorides are the two most important fluoride luminescent materials, which can be formed by the following two ways:

$$mAF + nREF_3 \rightarrow A_mRE_nF_{m+3n} \quad (A= \text{Alkalis metals; RE= Rare earth}) \quad (1)$$

$$mBF_2 + nREF_3 \rightarrow B_mRE_nF_{2m+3n} \quad (B= \text{Alkaline-earth metals; RE= Rare earth}) \quad (2)$$

Where m and n can be any one of natural numbers greater than zero. Therefore, by selecting and adjusting various ratios of $REF_3$ to metal fluoride, many novel rare earth fluoride compounds can be designed and obtained, such as $NaYF_4$ [16-18], $NaGdF_4$ [19-23], $BaYF_5$ [24-31], $BaGdF_5$ [32-41], $Ba_2GdF_7$ [42, 43] as well as $KY_3F_{10}$ [44-49]

etc. Recently, much attention has been paid to upconversion phenomenon in $AREF_4$ fluorides, especially for $NaYF_4$ [17, 18] and $NaGdF_4$ [20, 22] with particular interest, owing to their exceptional properties, both morphological (high monodispersity, small size of 5-20 nm, high crystallinity, possibility of surface modification) and spectroscopic (bright visible emission upon excitation, stable intensity over time).

Compared with the fluorides mentioned above, alkaline-earth lanthanide ternary fluorides have obtained relatively little attention, although they are excellent host materials that can be doped with divalent and trivalent lanthanide ions, which also exhibit the strong broadband emission in the near UV spectra region (360-440 nm) and highly efficient infrared- to-visible upconversion emission [25, 33, 35].

As an important kind of fluorides, $BaYF_5$ is particularly promising host for doping with $Ln^{3+}$ ions for UC fluorescence and Ba element has large K-edge value and high X-ray mass absorption coefficient. Moreover, $BaYF_5$ is also an ideal host for the $Yb^{3+}/Tm^{3+}$ codopants in nanoscale. Therefore, the research on $BaYF_5$ has been intensively carried out. However, the crystal phase of $BaYF_5$ is sensitive and polytropic with the variable synthesis conditions, there are mainly two types of crystals phase *i.e.* cubic and tetragonal according to the relative reports up to now. Nevertheless, a correlation between the synthesized phase and the luminescence behaviors is not clearly verified [50]. For example, cubic structure [24-27] and tetragonal structure [28-31] $BaYF_5$ micro/nano crystals have been synthesized by hydrothermal method.

Contrast to $BaYF_5$, another important compound with the general formula of

$BREF_5$ is $BaGdF_5$. Except that it is a good host matrix for luminescent $Ln^{3+}$ ions, $Gd^{3+}$ ion is also an ideal paramagnetic relaxation agent used in magnetic resonance imaging (MRI) because of its large magnetic moment and nanosecond time scale electronic relaxation time [32, 33, 37-41]. The seven unpaired inner 4f electrons of $Gd^{3+}$ ions are closely bound to the nucleus and can be effectively shielded from the crystal field by the outer closed-shell $5s^25p^6$ electrons, which gives rise to the magnetic properties of $Gd^{3+}$ ions. The magnetic moments related to $Gd^{3+}$ ions are all localized and non-interacting, which leads to the paramagnetism of $Gd^{3+}$ ions. This makes the $BaGdF_5$ a very attractive choice to be doped with various $Ln^{3+}$ ions to form single-phase multi-functional nanocrystals.

Non-stoichiometry of $Ba_xRE_yF_z$ compounds and many of crystal structures assigned to them have been investigated for many years [51-54]. The phase diagram of $BaF_2$-$REF_3$ system is complicated and reveals many phases and intermediate states [51]. The X-ray diffraction studies have shown that when the composition of fluoride is $Ba_{1-x}RE_xF_{2+x}$, a cubic crystal phase is formed with a fluorite-type structure, e.g. in $BaF_2$-$YF_3$ when $x< 0.36$ [54]. The structures of these compounds can easily distort from the ideal one [53]. What is more, M. Karbowiak *et al*. and P.P. Fedorov *et al*. have suggested that there is no such a phase as $BaYF_5$ and only $Ba_{1-x}Y_xF_{2+x}$ fluorides can be formed [50, 54, 55]. In present work we use the formula $BaREF_5$, instead of $Ba_{1-x}RE_xF_{2+x}$ as the compositions were similar to this molecular formula.

Attractively, can $BaYF_5$ and $BaGdF_5$ form $BaGd_{1-x}Y_xF_5$ ($0\leq x\leq 1.0$) continuous

solid solution? Can the replacement of $Gd^{3+}$ ion by $Y^{3+}$ ion influence the microstructures and UC luminescence of the formed $BaGd_{1-x}Y_xF_5$ solid solution host, and what are the influencing mechanisms? Obviously, once $Gd^{3+}$ ion was introduced into $BaYF_5$ host and formed solid solution, this novel polyfluoride contains $Gd^{3+}$ ion and $Y^{3+}$ ion will undoubtedly be an excellent multifunctional material possesses UC and DC luminescent properties and paramagnetism. Unfortunately, contrast to considerable researches on the unary $BaYF_5$ and $BaGdF_5$ nanocrystals [24-41], no report is concentrated on the synthesis, microstructures and upconversion (UC) luminescent properties of $BaGd_{1-x}Y_xF_5$ continuous solid solution up to now.

Motivated by the above mentioned interesting ideas, we have designed novel $BaGd_{1-x}Y_xF_5$ ($0\leq x\leq 1.0$) solid solution and synthesized $Ba(Gd_{1-x}Y_x)_{0.78}F_5$: 20 mol% $Yb^{3+}$, 2 mol% $Tm^{3+}$ ($0\leq x\leq 1.0$) solid solution nanocrystals via a facile hydrothermal method without using any organic solvent or chelating agent in the present work. Since the total concentration of Gd and Y in the host is invariant (78 mol%) and the doping level of Yb and Tm is fixed as 22 mol%, all the designed and synthesized co-doped solid solution nanocrystals were denoted as $Ba(Gd_{1-x}Y_x)_{0.78}F_5$: $Yb^{3+}$, $Tm^{3+}$ with various x ($0\leq x\leq 1.0$) in the following sections. Moreover, the influences of $Gd^{3+}$ concentration on the crystal phase, grain size, UC luminescent and magnetic properties of the obtained $Ba(Gd_{1-x}Y_x)_{0.78}F_5$: $Yb^{3+}$, $Tm^{3+}$ solid solution nanocrystals have been investigated in detail. In addition, the variation of UC luminescent properties and the mechanism of the upconversion process of the solid solution nanocrystals synthesized with different $Y^{3+}$ to

$Gd^{3+}$ molar ratios have also been studied. Our study will provide significant insights into the researches and applications on alkaline-earth lanthanide fluoride multifunctional nanocrystal phosphors.

## 2. Experimental section

### 2.1 Materials

All reagents were used directly without further purifications. Rare earth oxides $Y_2O_3$ (99.99%), $Gd_2O_3$ (99.99%), $Yb_2O_3$ (99.99%) and $Tm_2O_3$ (99.99%) were purchased from Shanghai Tongna Environmental Protection and Technology Co., Ltd. Analytical-grade barium nitrate ($Ba(NO_3)_2$), ammonium fluoride ($NH_4F$), ammonium hydroxide ($NH_3{\cdot}H_2O$), ethyl alcohol ($C_2H_5OH$) and nitric acid ($HNO_3$) were all received from Chengdu Kelong Glass Co., Ltd. Distilled water was used throughout the experiment.

### 2.2 Synthesis of $Ba(Gd_{1-x}Y_x)_{0.78}F_5$: $Yb^{3+}$, $Tm^{3+}$ solid solution nanocrystals

A series of rare $Ba(Gd_{1-x}Y_x)_{0.78}F_5$: $Yb^{3+}$, $Tm^{3+}$ solid solution nanocrystals were synthesized via a facile hydrothermal process without subsequent sintering treatment. In a typical synthesis procedure, the $Ln(NO_3)_3$ (Ln=Y, Gd, Yb, Tm) stock solution were initially prepared by dissolving the corresponding rare earth oxides in nitric acid by heating. According to the stoichiometric of the $Ba(Gd_{1-x}Y_x)_{0.78}F_5$: $Yb^{3+}$, $Tm^{3+}$ solid solution, and the corresponding demanded quantities of $Ln(NO_3)_3$, $Ba(NO_3)_2$ and $NH_4F$ solution were obtained. Firstly, a certain amount of $Ba^{2+}$ ions (as shown in Table 1) were added in a 100 mL beaker, after being stirred for about 0.5 h, $Ln(NO_3)_3$ solution

contained 3.9 mmol $Y^{3+}$ ions and $Gd^{3+}$ ions, 1.0 mmol $Yb^{3+}$ ions as well as 0.1 mmol $Tm^{3+}$ ions was added into the beaker successively, the mixture was thoroughly stirred for 0.5 h, then dilute solution contained 25 mmol $NH_4F$ was added dropwise into the beaker. Finally, the formed milk-like colloidal solution was transferred into a 100 mL Teflon-lined autoclave, and heated at 200 ℃ for 24 h. After being cooled to room temperature naturally, the final precipitates were centrifugally separated and collected at 3000 rpm for 30 min, washed with absolute ethyl alcohol and distilled water several times, respectively, and dried in air at 60 ℃ for 24 h. Thus, a series of $Ba(Gd_{1-x}Y_x)_{0.78}F_5$: $Yb^{3+}$, $Tm^{3+}$ solid solution nanocrystals were prepared.

**2.3 Characterization**

Powder X-ray diffraction (XRD) measurements were performed on a Rigaku SmartLab powder diffractometer with Cu K$\alpha$ radiation ($\lambda$=0.15406 nm) at a scanning rate of 4°/min in the 2$\theta$ range from 10° to 80°. The morphologies and sizes of the as-synthesized samples were performed on a JSM-7500 field emission scanning electron microscopy (FE-SEM), ZEISS Libra 200 FE transmission electron microscopy (TEM) and size distributions on Malvern Zetasizer Nano S (DLS). The electron energy-dispersive spectroscopy (EDS) elemental compositions were characterized by FEI Quanta 250 scanning electron microscope (SEM). The UC luminescent spectra of the obtained products were measured by using a Hitachi F-7000 fluorescence spectrophotometer equipped with a continuous 980 nm laser diode laser as the pump power source, the DC luminescent spectra were also performed on Hitachi F-7000

fluorescence spectrophotometer equipped with xenon lamp. The magnetic properties of the as-synthesized samples were characterized by Vibrating Sample Magnetometer (Versalab, Quantum Design Inc, USA). All measurements were performed at room temperature.

## 3. Results and discussion

### 3.1 Microstructure analysis

Fig. 1 shows the XRD patterns of the samples. It can be seen that all the as-synthesized crystals are highly crystalized, exhibiting all the corresponding strong diffraction peaks such as (111), (200), (220), (311) as well as (222), which are well consistent with cubic phase $BaGdF_5$ (JCPDS 24-0098) or cubic phase $BaYF_5$ (ICSD 169849), indicating that all the obtained $Ba(Gd_{1-x}Y_x)_{0.78}F_5$: $Yb^{3+}$, $Tm^{3+}$ crystals are continuous solid solutions possess pure cubic phase structure. This should be attributed to the same charge, similar radius and electronegativity of $Yb^{3+}$, $Tm^{3+}$, $Y^{3+}$ and $Gd^{3+}$ ions, and they can occupy the same lattice site in $BaGdF_5$ or $BaYF_5$ host. Moreover, all the observed diffraction peaks of $Ba(Gd_{1-x}Y_x)_{0.78}F_5$: $Yb^{3+}$, $Tm^{3+}$ crystals shifted to higher $2\theta$ side when $Gd^{3+}$ ions are replaced by $Y^{3+}$ ions gradually (*i.e.* x increased). To comparative observation, as an example, the enlarged XRD patterns in the range of 25-28° are also shown in Fig. 1 (right). In $Ba(Gd_{1-x}Y_x)_{0.78}F_5$: $Yb^{3+}$, $Tm^{3+}$ solid solution, $Gd^{3+}$ and $Y^{3+}$ have the same coordination number (CN = 8) and occupy the same lattice site, and the radius of $Gd^{3+}$ ion (1.053 Å) in the eight coordination is a little larger than that of $Y^{3+}$ ion (1.019 Å) [56]. Obviously, according to Bragg's equation ($n\lambda=2d\sin\theta$),

the lattice parameters of the unit cell of the $Ba(Gd_{1-x}Y_x)_{0.78}F_5$: $Yb^{3+}$, $Tm^{3+}$ solid solution will decrease with the increasing x, and thus leading the diffraction peaks shifted to higher $2\theta$ side. To further investigate the detailed crystal structural evolution on the substitution of $Y^{3+}$ ions in the crystal lattice, the Rietveld refinement was performed on the program GSAS_EXPGUI. As shown in Fig. 2, all the obtained crystals are fitted well with cubic phase of $BaYF_5$ (ICSD 169849), and the refined structural parameters and good refined factors ($R_{wp}$, $R_p$ and $\chi^2$) are shown in Table 2. One can see that the lattice parameters of the cubic phase $Ba(Gd_{1-x}Y_x)_{0.78}F_5$: $Yb^{3+}$, $Tm^{3+}$ decrease with increasing concentration of $Y^{3+}$ ions, which is well accordant with the XRD results.

We further studied the general morphology and size evolution of $Ba(Gd_{1-x}Y_x)_{0.78}F_5$: $Yb^{3+}$, $Tm^{3+}$ crystals substituted with different amount of $Y^{3+}$ through field emission scanning electron microscopy (FE-SEM), as shown in Fig. 3. It can be found that all the obtained crystals are quasi-spherical nanocrystals with diameters ranging from ~55 nm to ~240 nm, implying that the introduction of $Y^{3+}$ into the $BaGdF_5$ host cannot change the morphology of the formed $Ba(Gd_{1-x}Y_x)_{0.78}F_5$: $Yb^{3+}$, $Tm^{3+}$ solid solution crystals whereas significantly influence their grain size. Moreover, the grain size of the solid solution nanocrystals decreases with the increasing amount of $Y^{3+}$ ions, indicating that the doping of $Y^{3+}$ ion can inhibit the grain growth, and such small grain size can ensure that the as-synthesized $Ba(Gd_{1-x}Y_x)_{0.78}F_5$: $Yb^{3+}$, $Tm^{3+}$ solid solution nanocrystals are potential to be used in bio-imaging. To more clearly exhibit the changes in crystallite size, the transmission electron microcopy (TEM) and size distribution measurements

were performed. As some examples, Fig.4 gives the TEM images of the selected $Ba(Gd_{1-x}Y_x)_{0.78}F_5$: $Yb^{3+}$, $Tm^{3+}$ nanocrystals with x=0, x=0.2, x=0.4, x=0.6, x=0.8 and x=1.0, respectively. The histogram plots of $Ba(Gd_{1-x}Y_x)_{0.78}F_5$: $Yb^{3+}$, $Tm^{3+}$ nanocrystals and dependencies of mean grain size on the concentration of $Y^{3+}$ ion are also shown in Fig. 5. Relative homodisperse $Ba(Gd_{1-x}Y_x)_{0.78}F_5$: $Yb^{3+}$, $Tm^{3+}$ nanocrystals with quasi-spherical shapes can be seen in TEM images, and the crystallite size gradually decreases with the increasing x (seen in the inset of each image), which is in accordance with SEM results. Fig. 5 reveals that the mean grain size of the as-synthesized $Ba(Gd_{1-x}Y_x)_{0.78}F_5$: $Yb^{3+}$, $Tm^{3+}$ nanocrystals slightly decreased from ~240 nm to ~223 nm when x increased from 0 to 0.6. However, when $0.7 \leq x \leq 1.0$, the mean grain size of the nanocrystals markedly decreases with further increasing x (from ~200 nm to ~55 nm). Obviously, at the lower concentration of $Gd^{3+}$ ion (*i.e.* $x \geq 0.7$), the doping of $Y^{3+}$ can notably inhibit the growth of the final $Ba(Gd_{1-x}Y_x)_{0.78}F_5$: $Yb^{3+}$, $Tm^{3+}$ nanocrystals. T. Grzyb *et al*. also have found that the size of the microwave hydrothermal synthesized $BaREF_5$ (RE= Y, Gd and Lu) increases gradually with the atomic number of $RE^{3+}$ ion from $Y^{3+}$ to $Gd^{3+}$ to $Lu^{3+}$ [57]. Although the exact mechanism is unclear, we may give the plausible explanation as follows.

According to our previous work [20], the formation of the $BaGd_{1-x}Y_xF_5$ solid solution crystals also may be summarized as follows:

$$(1-x)Gd^{3+} + xY^{3+} + 3F^- \rightarrow Gd_{1-x}Y_xF_3 \quad \text{(crystal)} \qquad (3)$$

$$Gd_{1-x}Y_xF_3\ \text{(crystal)} + 2F^- + Ba^{2+} \rightarrow BaGd_{1-x}Y_xF_5 \quad \text{(crystal)} \qquad (4)$$

Generally speaking, the nucleation rate of crystal nucleus will have significantly influence on the particle size of the final crystals in solution system. The larger the nucleation rate of crystal nucleus, the smaller the particle size of the final crystals will be. In our case, the obtained $BaGdF_5$:$Yb^{3+}$, $Tm^{3+}$ and $BaYF_5$: $Yb^{3+}$, $Tm^{3+}$ nanocrystals have distinct difference in average particle size (~240 nm and ~55 nm, respectively), and this may be attributed to the greater nucleation rate of $BaYF_5$: $Yb^{3+}$, $Tm^{3+}$ nanocrystals than that of $BaGdF_5$:$Yb^{3+}$, $Tm^{3+}$ nanocrystals under the same hydrothermal conditions. Therefore, the grain size of the final $Ba(Gd_{1-x}Y_x)_{0.78}F_5$: $Yb^{3+}$, $Tm^{3+}$ nanocrystals should be determined by the dominant constituent (*i.e.* $BaGdF_5$ or $BaYF_5$). It can be reasonably concluded that the nucleation rate of $Ba(Gd_{1-x}Y_x)_{0.78}F_5$: $Yb^{3+}$, $Tm^{3+}$ nanocrystals will increase with the increasing content of $BaYF_5$ (*i.e.* x), leading to the decrease of the grain size for the final $Ba(Gd_{1-x}Y_x)_{0.78}F_5$: $Yb^{3+}$, $Tm^{3+}$ nanocrystals accordingly.

In addition, in order to evaluate whether the chemical composition in the obtained $Ba(Gd_{1-x}Y_x)_{0.78}F_5$: $Yb^{3+}$, $Tm^{3+}$ solid solution nanocrystals are consistent with that of starting solution, EDS were used to detect the atomic percentage of the ions in the samples, and the results are shown in Fig. 6 and Table 3, respectively. All the obtained samples present the characteristic diffraction peaks of all the chemical elements in the designed $Ba(Gd_{1-x}Y_x)_{0.78}F_5$: $Yb^{3+}$, $Tm^{3+}$ solid solution, and the molar ratio of $Ba^{2+}$: $RE^{3+}$ is very close to 1:1. Especially, the molar ratio of Y to Gd is almost accord with the value of x in the starting solution. Combination with the XRD results, we can confirm

that all the obtained final samples are really $Ba(Gd_{1-x}Y_x)_{0.78}F_5$: $Yb^{3+}$, $Tm^{3+}$ solid solution crystals. As an example, Fig. 7 shows the element mapping of Gd, Y, Yb and Tm of the as-synthesized $Ba(Gd_{0.2}Y_{0.8})_{0.78}F_5$: $Yb^{3+}$, $Tm^{3+}$ solid solution crystal. It is clearly that all the rare- earth elements in the crystals are equally distributed in the solid solution.

**3.2 Photoluminescence properties**

Fig. 8 presents the PL spectra of the $Ba(Gd_{1-x}Y_x)_{0.78}F_5$: $Yb^{3+}$, $Tm^{3+}$ nanocrystals under excitation with 980 nm near-infrared light. The inset shows the dependence of the $Y^{3+}$ substitution concentration (*i.e.* x) on the maximal intensity (peak at 478 nm) of the UC luminescence. All samples exhibit main blue emission centered at 478 nm ascribed to $^1G_4 \rightarrow {}^3H_6$ transition of $Tm^{3+}$ ions, and a series of weak UC emissions including ultraviolet (UV, ~360 nm), red (~630 nm), near infrared (~680 nm) and (~765 nm), originating from the $^1D_2 \rightarrow {}^3H_6$, $^1G_4 \rightarrow {}^3F_4$, $^3F_3 \rightarrow {}^3H_6$ and $^3H_4 \rightarrow {}^3H_6$ transition of $Tm^{3+}$ ions respectively. It also can be seen that with increasing $Y^{3+}$ substitution concentrations in the $BaGdF_5$ host lattice, all the peak positions of the UC luminescence spectra for the obtained $Ba(Gd_{1-x}Y_x)_{0.78}F_5$: $Yb^{3+}$, $Tm^{3+}$ solid solution nanocrystals are unchanged, whereas their UC emission intensity (peak at 478 nm) initially increases and then notably decreases with increasing content of $Y^{3+}$ ion, giving the maximum at x=0.8. Interestingly, as also shown in the inset of Fig. 8, after a little $Gd^{3+}$ ion being replaced by $Y^{3+}$ ion, the UC emission intensities (peak at 478 nm) of the formed $Ba(Gd_{1-x}Y_x)_{0.78}F_5$: $Yb^{3+}$, $Tm^{3+}$ solid solution nanocrystals are greater than the as-synthesized co-doped pure $BaGdF_5$ and $BaYF_5$ nanocrystals. Particularly, when x is

0.6, 0.7, 0.8 and 0.9, the enhancement degree of the blue emission intensity for the $Ba(Gd_{1-x}Y_x)_{0.78}F_5$: $Yb^{3+}$, $Tm^{3+}$ nanocrystals is more significant than that of the co-doped nanocrystals with the other x values. These results indicate that the UC luminescence properties of the $Ba(Gd_{1-x}Y_x)_{0.78}F_5$: $Yb^{3+}$, $Tm^{3+}$ series nanocrystals can be effectively modulated through the replacement of $Gd^{3+}$ ions by $Y^{3+}$ ions.

In general, the chemical composition, microstructures (morphology and grain size) and crystal symmetry of the luminescent crystal are the three key roles that determine its UC luminescence property. Actually, the UC luminescence emission intensity of the obtained $Ba(Gd_{1-x}Y_x)_{0.78}F_5$: $Yb^{3+}$, $Tm^{3+}$ nanocrystals may be attributed to the following two aspects in our case.

On the one hand, the UC emission intensity of the $Ba(Gd_{1-x}Y_x)_{0.78}F_5$: $Yb^{3+}$, $Tm^{3+}$ nanocrystals is mainly dependent on the effective content of $BaYF_5$ host in the solid solution, since $BaYF_5$ is acknowledged as one of the most efficient UC host materials. Therefore, the substitution concentration of $Y^{3+}$ (in fact, the effective content of $YF_3$ host) has a remarkable influence on the UC emission intensity of the $Ba(Gd_{1-x}Y_x)_{0.78}F_5$: $Yb^{3+}$, $Tm^{3+}$ nanocrystals. In other words, the UC emission intensity of the $Ba(Gd_{1-x}Y_x)_{0.78}F_5$: $Yb^{3+}$, $Tm^{3+}$ nanocrystals will increase with increasing x (*i.e.* concentration of $YF_3$) if the other influencing factors are ignored. Because there is no effective $YF_3$ host, the as-synthesized pure $BaGd_{0.78}F_5$: $Yb^{3+}$, $Tm^{3+}$ nanocrystal possesses the lowest UC luminescence emission intensity compared with the other $Ba(Gd_{1-x}Y_x)_{0.78}F_5$: $Yb^{3+}$, $Tm^{3+}$ nanocrystals ($0.1 \leq x \leq 0.9$), even if it has the largest

average particle size.

On the other hand, the grain size of the sample also affects the UC luminescence intensity since the relative intensity of upconverted emissions changes with the surface concentration quenching effect [58-60]. As the particle size decreases, the concentration of the surface dopant ions increases with the bigger surface-to-volume ratio, leading to a softened variation of the relative emission intensity [61]. Since the gross of Yb and Tm is a fixed value and the molar ratio of Yb to Tm is unchanged, the relative concentration of Yb and Tm in the unit volume will increase with the decrease of lattice constant of $Ba(Gd_{1-x}Y_x)_{0.78}F_5$: $Yb^{3+}$, $Tm^{3+}$ nanocrystals. That is to say there are more Yb and Tm ions in each unit volume, this may lead the increase of effective concentration of Yb and Tm ions and further enhance or decrease (concentration quenching effect) the intensity of UC luminescence.

Clearly, the UC emission intensity of $Ba(Gd_{1-x}Y_x)_{0.78}F_5$: $Yb^{3+}$, $Tm^{3+}$ nanocrystals should be determined by the comprehensive influences of the above mentioned two aspects. At the lower substitution concentration of $Y^{3+}$ ion ($0 \leq x \leq 0.3$), the effective content of $YF_3$ host in the $Ba(Gd_{1-x}Y_x)_{0.78}F_5$: $Yb^{3+}$, $Tm^{3+}$ solid solution nanocrystals is relative low, so their UC emission intensity slightly lift with the increasing x. Although the gradually increase of doped $Y^{3+}$ (*i.e.* x) will increase the content of $YF_3$ host in the $Ba(Gd_{1-x}Y_x)_{0.78}F_5$ solid solution nanocrystals and enhance their UC emission intensity, it also leads the significantly decrease in grain size of the $Ba(Gd_{1-x}Y_x)_{0.78}F_5$: $Yb^{3+}$, $Tm^{3+}$ solid solution nanocrystals and drastically weakens their UC emission intensity in such

conditions. In other words, the enhancement of UC luminescence comes from the increase of the effective content of $BaYF_5$ (*i.e.* the effective content of $YF_3$) host moderately exceeds the reduction of UC luminescence stems from the decrease in grain size. On the whole, the UC emission intensities of $Ba(Gd_{1-x}Y_x)_{0.78}F_5$: $Yb^{3+}$, $Tm^{3+}$ solid solution nanocrystals gently increase with the increasing x and a little higher than that of the as-synthesized pure $BaGdF_5$ and $BaYF_5$ nanocrystals.

When $0.4 \leq x \leq 0.8$, the concentration of $YF_3$ is high enough, and the enhancement of UC luminescence comes from the increase of the effective content of $YF_3$ in the solid solution is much higher than the reduction of UC luminescence stems from the decrease in grain size. As a result, the UC emission intensities of the co-doped $Ba(Gd_{1-x}Y_x)_{0.78}F_5$ solid solution nanocrystals sharply increase with the increasing x. Whereas when $x>0.8$, the UC emission intensities of the co-doped nanocrystals solid solution nanocrystals abruptly decrease with the further increasing x, this may be attributed to the concentration quenching effect comes from the increase of effective concentration of Yb and Tm ions in each unit volume owing to the decrease of lattice constant of $Ba(Gd_{1-x}Y_x)_{0.78}F_5$: $Yb^{3+}$, $Tm^{3+}$ nanocrystals accordingly. As for the as-synthesized pure $BaY_{0.78}F_5$: $Yb^{3+}$, $Tm^{3+}$ nanocrystal, the smallest average particle size leads to the strongest concentration quenching effect although it has the largest effective content of $YF_3$ host. As a result, it also presents the much lower UC emission intensity.

In order to study the UC luminescence mechanism, the excitation power-dependent UC emissions intensities of $Ba(Gd_{1-x}Y_x)_{0.78}F_5$: $Yb^{3+}$, $Tm^{3+}$ nanocrystals were measured,

as shown in Fig. 9. For the unsaturated UC process, the number of photons which are required to populate the upper emitting level can be described by the following relation [62]:

$$I_f \propto P^n$$

Where $I_f$ is the upconversion emission intensity, $P$ is the laser pump power and $n$ is the number of the laser photons involved. More specifically, an emission band that demands $n$ energy transfer upconversion steps to be excited will have a slope of $n$ when the UC luminescence intensity is double-logarithmically plotted *versus* pump power used [63]. As can be seen, the slope value (*i.e.* $n$) for the emission peak located at 478 nm and 630 nm are 2.30 and 1.84, respectively. This result indicates that $^1G_4 \rightarrow {}^3H_6$ and $^1G_4 \rightarrow {}^3F_4$ transitions of $Tm^{3+}$ ion originate from a three-photon and two-photon processed, respectively.

As one of the most commonly used activators, it is well established that $Tm^{3+}$ ions are of greater interest and more applicable in biomedical diagnostics, high-density optical data storage and reading and photoprinting since their two stable levels, *i.e.* $^1G_4$ and $^3F_4$, and blue UC luminescence near 480 nm [64, 65].

The upconversion mechanism is shown in Fig. 10. Under 980 nm near-infrared light excitation, $Yb^{3+}$ ions are excited from the ground state $^2F_{7/2}$ to the excited state $^2F_{5/2}$ rapidly because $Yb^{3+}$ ion has a large absorption cross section around 980 nm, and then $Yb^{3+}$ ions decays to the ground state and at the meanwhile, the absorbed energy transferred to $Tm^{3+}$ ions efficiently. The uninterrupted energy transitions between $Yb^{3+}$

ions and $Tm^{3+}$ ions make $Tm^{3+}$ ions transferred from $^3H_6$ to $^1G_4$ level and $^3F_{2,3}$ levels, at the $^1G_4$ level, the $Tm^{3+}$ can non-radiative decay to the $^3H_6$, $^3F_4$ levels, yield the blue and red emissions respectively. Moreover, there is an energy transition process between $Gd^{3+}$ ion and $Tm^{3+}$ ions as shown in Fig. 10, when the $^1D_2$ energy level of $Tm^{3+}$ is pumped to $^1I_6$ energy level, then the energy of this excited state transfer to $^6P_{7/2}$ energy level of $Gd^{3+}$ ion, which is also seen in Refs. [66, 67]. Fig. 11 is the CIE chromaticity diagram for the emission spectrum of $Ba(Gd_{0.2}Y_{0.8})_{0.78}F_5$: $Yb^{3+}$, $Tm^{3+}$ nanocrystal (*i.e.* x=0.8), we can see that the sample yields pure blue light and gives the chromaticity coordinates at (0.1586, 0.1250), which will be a promising blue light resource. The investigation on the down conversion (DC) luminescence properties of the synthesized $Ba(Gd_{1-x}Y_x)_{0.78}F_5$: $Yb^{3+}$, $Tm^{3+}$ nanocrystals are given in supporting information (Fig. S1 and Fig. S2).

**3.3 Paramagnetic property**

The inorganic compounds containing $Gd^{3+}$ generally exhibit paramagnetic properties for the seven unpaired inner 4*f* electrons, which is well protected by the outer $5s^25p^6$ electrons. Hence, the as-synthesized $Ba(Gd_{1-x}Y_x)_{0.78}F_5$: $Yb^{3+}$, $Tm^{3+}$ nanocrystals not only exhibit excellent luminescent properties, but also show magnetic properties when applied magnetic field. Fig. 12 shows the hysteresis loops of $Ba(Gd_{1-x}Y_x)_{0.78}F_5$: $Yb^{3+}$, $Tm^{3+}$ ($0 \leq x \leq 0.9$) nanocrystals at room temperature (300 K). One can see that all the samples present benign paramagnetism in the magnetic range of -30 to 30 kOe at 300 K due to no coercivity or no remanence. Moreover, the observed magnetization of

$Ba(Gd_{1-x}Y_x)_{0.78}F_5$: $Yb^{3+}$, $Tm^{3+}$ ($0 \leq x \leq 0.9$) solid solution nanocrystals gradually decreases from 1.77 to 0.34 emu/g when x increases from 0 to 0.9 (inset of Fig. 12), this should be ascribed to the continuous reduction of the magnetic composition content (*i.e.* the concentration of $GdF_3$) for the obtained co-doped nanocrystals, and our results are also similar to the previous reports [36, 38, 39].

**4. Conclusion**

In summary, $Ba(Gd_{1-x}Y_x)_{0.78}F_5$: 20 mol% $Yb^{3+}$, 2 mol% $Tm^{3+}$ ($0 \leq x \leq 1.0$) continuous solid solution nanocrystals with single cubic phase structure have been synthesized through a facile hydrothermal method. The microstructures, UC luminescent and magnetic properties of the obtained $Ba(Gd_{1-x}Y_x)_{0.78}F_5$: $Yb^{3+}$, $Tm^{3+}$ solid solution nanocrystals have been significantly impacted by the concentration of $Y^{3+}$ ions. The UC emission intensity (peak at 478 nm) initially increases with increasing content of $YF_3$ and then notably decreases, giving the maximum at x=0.8, and this should be attributed to the synergistic effect of the content of the main effective UC host and the microstructures of the co-doped nanocrystals. $Ba(Gd_{1-x}Y_x)_{0.78}F_5$: $Yb^{3+}$, $Tm^{3+}$ ($0.4 \leq x \leq 0.8$) nanocrystals are demonstrated to be better host matrixes than pure $BaYF_5$ and/or $BaGdF_5$ for UC luminescence, and the $Ba(Gd_{0.2}Y_{0.8})_{0.78}F_5$: $Yb^{3+}$, $Tm^{3+}$ nanocrystals (*i.e.* x=0.8) owns highest UC fluorescent efficiency. Moreover, all the obtained $Ba(Gd_{1-x}Y_x)_{0.78}F_5$: $Yb^{3+}$, $Tm^{3+}$ solid solution nanocrystals exhibit benign paramagnetism at room temperature, showing the potential applications in displays, biological labels and bio-separations. Our present work may provide a guidance to

design and synthesize the other fluoride solid solution systems with superior UC luminescence properties and more promising applications.

**Acknowledgements**

This work was supported by the National Science Foundation of China (NSFC, No. 51551202), the Scientific Research Fund of Sichuan Provincial Education Department (16TD0007, 15ZA0363 and 12ZA142), the Applied Basic Research Fund of Science & Technology Department of Sichuan Province (No. 2015JY0274), and the Scientific Research Fund of Sichuan Normal University (No. DJ2016-22, DJ2016-26 and DJ2016-27).

**References**

[1] N. Niu, P.P. Yang, Y.C. Liu, C.X. Li, D. Wang, S.L. Gai, F. He, J. Colloid Interface Sci. 362 (2011) 389-396.

[2] H.J. Na, J.S. Jeong, H.J. Chang, H.Y. Kim, K.J. Woo, K.P. Lim, K.A. Mkhoyan, H.S. Jang, Nanoscale 6 (2014) 7461-7468.

[3] Z.M. Xiong, Y.S. Yang, Y.F. Wang, RSC Adv. 6 (2016) 75664-75668.

[4] S Sarkar, V.N.K.B. Adusumalli, V. Mahalingam, J.A. Capobianco, PCCP. 17 (2015) 17577-17583.

[5] G. Anjaiah, SK. Nayab Rasool, P. Kistaiah, J. Lumin. 159 (2015) 110-118.

[6] R.K. Sharma, A.V. Mudring, P. Ghosh, J. Lumin. 189 (2017) 44-63.

[7] S. Kundu, A. Kar, A. Patra, J. Lumin. 132 (2012) 1400-1406.

[8] P.A. Loiko, N.M. Khaidukov, J. Méndez-Ramos, E.V. Vilejshikova, N.A. Skoptsov, K.V. Yumashev, J. Lumin. 170 (2016) 1-7.

[9] S.H. Pan, R.P. Deng, J. Feng, S.Y. Song, S. Wang, M. Zhu, H.J. Zhang, Cryst. Eng. Comm. 15 (2013) 7640-7643.

[10] H.L. Qiu, G.Y. Chen, L. Sun, S.W. Hao, G. Han, C.H. Yang, J. Mater. Chem. 21 (2011) 17202-17208.

[11] C. M. Zhang, P.A. Ma, C.X. Li, S.S. Huang, D.M. Yang, M.M. Shang, X.J. Kang, J. Lin, J. Mater. Chem. 21 (2011) 717-723.

[12] C.L. Chen, J.H. Liu, Y. Chen, C.G. Li, X.M. Liu, H. Huang, C. Liang, Y. Lou, Z. Shi, S.H. Feng, Appl. Mater. Interfaces 9 (2017) 5748-5756.

[13] J. Xu, S.L. Gai, Y.L. Dai, G.X. Yang, F. He, P.P. Yang, J. Mater. Chem B 2 (2014) 1791-1801.

[14] L.W. Yang, Y.Y. Zhang, J.J. Li, J.X. Zhong, P.K. Chu, Nanoscale 2 (2010) 2805-2810.

[15] B. Zhou, B.Y. Shi, D.Y. Jin, X.G. Liu, Nature nanotech. 10 (2015) 924-936.

[16] I.Z. Dinic, L.T. Mancic, M.E. Rabanal, K. Yamamoto, S. Ohara, S. Tamura, T. Koji, A.M.L.M. Costa, B.A. Marinkovic, O.B. Milosevic, Adv. Powder Technol. 28 (2017) 73-82.

[17] A. Pilch, D. Wawrzyńczyk, M. Kurnatowska, B. Czaban, M. Samoć, W. Strek, A.

Bednarkiewicz, J. Lumin. 182 (2017) 114-122.

[18] Y.Q. Wu, Y. Ji, J. Xu, J.J. Liu, Z.W. Lin, Y.L. Zhao, Y. Sun, L. Xu, K.J. Chen, Acta Mater. 131 (2017) 373-379.

[19] D. Li, Q.L. Ma, X. Xi, X.T. Dong, W.S. Yu, J.X. Wang, G.X. Liu, Chem. Eng. J. 309 (2017) 230-239.

[20] T. Zhou, X.J. Jiang, C. Zhong, X.X. Tang, S.S. Ren, Y. Zhao, M.J. Liu, X. Lai, J. Bi, D.J. Gao, J. Lumin. 175 (2016) 1-8.

[21] X.H. Chuai, X.Y. Guo, X.H. Liu, G.H. He, K.Z. Zheng, C.F. He, W.P. Qin, Opt. Mater. 44 (2015) 13-17.

[22] C.Y. Liu, Z.Y. Gao, J.F. Zeng, Y. Hou, F. Fang, Y.L. Li, R.R. Qiao, L. Shen, H. Lei, W.S. Yang, M.Y. Gao, ACS Nano. 7 (2013) 7227-7240.

[23] D. Wang, L. Ren, X. Zhou, X.Z. Wang, J. Zhou, Y. Han, N. Kang, Nanotech, 23 (2012) 225705-225714.

[24] Y.J. Huang, H.P. You, G. Jia, Y.H. Song, Y.H. Zheng, M. Yang, K. Liu, N. Guo, J. Phys. Chem. C 114 (2010) 18051-18058.

[25] T. Grzyb, S. Balabhadra, D. Przybylska, M.W. cławiak. J. Alloys Compd. 649 (2015) 606-616.

[26] C.L. Chen, C.G. Li, L. Zhao, X.M. Liu, T.Y. Bai, H. Huang, Z. Shi, S.H. Feng. Inorg. Chem. Commum. 62 (2015) 11-14.

[27] M. Ma, L.W. Yang, G.Z. Ren, C.F. Xu, J.G. Lin, Q.B. Yang, J. Alloys Compd. 131 (2011) 1482-1486.

[28] J.Y. Sun, J.B. Xian, X.Y. Zhang, H.Y. Du, J. Alloys Compd. 509 (2011) 2348-2354.

[29] H.Y. Du, W.H. Zhang, J.Y. Sun, J. Alloys Compd. 509 (2011) 3413-3418.

[30] J.Y. Sun, J.B. Xian, H.Y. Du, J. Phys. Chem. Solids 72 (2011) 207-213.

[31] P. Haritha, I.R. Martín, C.S.D. Viswanath, N. Vijaya, K.V. Krishnaiah, C.K. Jayasankar, D. Haranath, V. Lavín, V. Venkatramu, Opt. Mater. 70 (2017) 16-24.

[32] H.L. Li, G.X. Liu, J.X. Wang, X.T. Dong, W.S. Yu, J. Lumin. 186 (2017) 6-15.

[33] Q. Zhao, Z. Lei, S. Huang, X.L. Han, B.Q. Shao, W. Lü, Y.C. Jia, W.Z. Lv, M.M. Jiao, Z.X. Wang, H.P. You, Appl. Mater. Interfaces 6 (2014) 12761-12770.

[34] H.X. Guan, Y.H. Song, P.C. Ma, M.Q. Chang, J. Chen, Y.X. Wang, B. Yuan, H.F. Zou, RSC Adv. 6 (2016) 53444-53453.

[35] D.M. Yang, X.J. Kang, M.M. Shang, G.G. Li, C. Peng, C.X. Li, J. Lin, Nanoscale 3 (2011) 2589-2595.

[36] C.M. Zhang, J.Y. Wang, C.Y. Song, Y.L. Shang, S.G. Shen, Mater. Lett. 118 (2014) 88-91.

[37] F. He, C.X. Li, X.Y. Zhang, Y.Y. Chen, X.R. Deng, B. Liu, Z. Y. Hou, S.S. Huang, D.Y. Jin, J. Lin, Dalton Trans. 45 (2016) 1708-1716.

[38] H.X. Guan, Y.H. Song, K.Y. Zheng, Y. Sheng, H.F. Zou, PCCP. 18 (2016) 13861-13873.

[39] H.X. Guan, Y. Sheng, Y.H. Song, K.Y. Zheng, C.Y. Xu, X.M. Xie, Y.Z. Dai, H.F. Zou, RSC Adv. 6 (2016) 73160-73169.

[40] X.Y. Huang, L. Jiang, X.X. Li, A.Q. He, J. Alloys Compd. 721 (2017) 374-382.

[41] D.M. Yang, Y.L. Dai, J.H. Liu, Y. Zhou, Y.Y. Chen, C.X. Li, P.A. Ma, J. Lin, Biomater. 35 (2014) 2011-2023.

[42] H.L. Li, G.X. Liu, J.X. Wang, X.T. Dong, W.S. Yu, New J. Chem. 41 (2017) 1609-1617.

[43] H.L. Li, G.X. Liu, J.X. Wang, X.T. Dong, W.S. Yu, J. Colloid Interface Sci. 501 (2017) 215-221.

[44] M. Runowski, J. Lumin. 186 (2017) 199-204.

[45] S. Goderski, M. Runowski, S. Lis, J. Rare Earths 34 (2016) 808-813.

[46] A. Grzechnik, K. Friese, Solid State Sci. 30 (2014) 61-67.

[47] L. Gomes, H.M. Silva, M.D. Linhares, R.U. Ichikawa, L.G. Martinez, I.M. Ranieri, J. Lumin. 157 (2015) 285-292.

[48] L. Gomes, H.M. Silva, M.D. Linhares, R.U. Ichikawa, L.G. Martinez, S.L. Baldochi, Opt. Mater. 54 (2016) 57-66.

[49] L. Zhu, Y.J. Liu, X.Z. Fan, D.W. Yang, X.Q. Cao, J. Lumin. 131 (2011) 1380-1385.

[50] M. Karbowiak, J. Cichos, J. Alloys Compd. 673 (2016) 258-264.

[51] R.J.M. Konings, A.Kovács, Handbook on the Physics and Chemistry of Rare Earths, vol. 33, Elsevier, Amsterdam, 2003, pp. 147-247.

[52] A. M. Golubev, L.P. Otroshchenko, V.N. Molchanov, B.P. Sobolev, Crystallogr. Rep. 53 (2008) 966-973.

[53] B.P. Sobolev, A.M. Golubev, E.A. Krivandina, M.O. Marychev, E.V. Chuprunov, X. Alcobe, Crystallogr. Rep. 47 (2002) 201-212.

[54] P.P. Fedorov, M.N. Mayakova, S.V. Kuznetsov, V.V. Voronov, R.P. Ermakov, K.S. Samarina, A. I. Popov, V. V. Osiko, Mater. Res. Bull. 47 (2012) 1794-1799,

[55] P. P. Fedorov , A. A. Luginina, S. V. Kuznetsov, V. V. Osiko, J. Fluorine Chem. 132 (2011) 1012-1039.

[56] R.D. Shannon, Acta Cryst. 32 (1976) 751-767.

[57] T. Grzyb, S. Balabhadra, D. Przybylska, M. Węcławiak, J. Alloys Compd. 649 (2015) 606-616.

[58] F. Wang, Y. Han, C.S. Lim, Y.H. Lu, J. Wang, J. Xu, H.Y. Chen, C. Zhang, M.H. Hong, X.G. Liu, Nature 463 (2010) 1061-1065.

[59] F. Wang, J. Wang, X.G. Liu, Angew. Chem.-Int. Edit. 122 (2010) 7618-7622.

[60] Y.C. Jiao, X.Y. Gao, J.X. Lu, Y.S. Chen, W. He, X.M. Chen, X.L. Li, R. Li, J. Alloys Compd. 549 (2013) 245-253.

[61] F. Shi, J.S. Wang, D.S. Zhang, G.S. Qin, W.P. Qin, J. Mater. Chem. 21 (2011) 13413-13421.

[62] G.Y. Chen, H.C. Liu, G. Somesfalean, H.J. Liang, Z.G. Zhang, Nanotech. 20 (2009) 385704-385709.

[63] J.F. Suyver, A. Aebischer, S.G. Revilla, P. Gerner, H.U. Güdel, Phys. Rev. B. 71 (2005) 125123-125131.

[64] F. Vetrone, V. Mahalingam, J.A. Capobianco, Chem. Mater. 21 (2009) 1847-1851.

[65] S.G. Xiao, X.L. Yang, J.W. Ding, X.H. Yan, J. Phys. Chem. C 111 (2007) 8161-8165.

[66] X.W. Zhang, Z. Zhao, X. Zhang, D.B. Cordes, B. Weeks, B.S. Qiu, K. Madanan, D. Sardar, J. Chaudhuri, Nano Res., 8 (2015) 636-648.

[67] K.Z. Zheng, Z.Y. Liu, C.J. Lv, W.P. Qin, J. Mater. Chem. C 1 (2013) 5502-5507.

## Table Captions

Table. 1 Overview of the hydrothermal conditions of controllable synthesis of $Ba(Gd_{1-x}Y_x)_{0.78}F_5$: $Yb^{3+}$, $Tm^{3+}$ solid solution nanocrystals.

Table. 2 Rietveld refinement patterns of the $Ba(Gd_{1-x}Y_x)_{0.78}F_5$: $Yb^{3+}$, $Tm^{3+}$ nanocrystals.

Table. 3 Atomic percentage of the synthesized $Ba(Gd_{1-x}Y_x)_{0.78}F_5$: $Yb^{3+}$, $Tm^{3+}$ solid solution nanocrystals.

## Figure Captions

Fig. 1 XRD patterns of $Ba(Gd_{1-x}Y_x)_{0.78}F_5$: $Yb^{3+}$, $Tm^{3+}$ solid solution nanocrystals (left side) and the enlarged patterns in the $2\theta$ range from 25° to 28° (right side).

Fig. 2 XRD refinements of the $Ba(Gd_{1-x}Y_x)_{0.78}F_5$: $Yb^{3+}$, $Tm^{3+}$ nanocrystals.

Fig. 3 FE-SEM characterization of $Ba(Gd_{1-x}Y_x)_{0.78}F_5$: $Yb^{3+}$, $Tm^{3+}$ solid solution nanocrystals.

Fig. 4 TEM images of the selected $Ba(Gd_{1-x}Y_x)_{0.78}F_5$: $Yb^{3+}$, $Tm^{3+}$ solid solution nanocrystals: (a) x=0, (b) x=0.2, (c) x=0.4, (d) x=0.6, (e) x=0.8, (f) x=1.0.

Fig. 5 Histogram plots of $Ba(Gd_{1-x}Y_x)_{0.78}F_5$: $Yb^{3+}$, $Tm^{3+}$ solid solution nanocrystals (a-k) and dependencies of mean grain size on the concentration of $Y^{3+}$ ion (l).

Fig. 6 EDS spectra of $Ba(Gd_{1-x}Y_x)_{0.78}F_5$: $Yb^{3+}$, $Tm^{3+}$ solid solution nanocrystals.

Fig. 7 Element mapping images of Gd, Y, Yb, Tm in $Ba(Gd_{0.2}Y_{0.8})_{0.78}F_5$: $Yb^{3+}$, $Tm^{3+}$ (x=0.8) correspond to the EDS region.

Fig. 8 UC emission spectra of $Ba(Gd_{1-x}Y_x)_{0.78}F_5$: $Yb^{3+}$, $Tm^{3+}$ nanocrystals under 980 nm

laser diode pump at room temperature 101.26 mW.

Fig. 9 Double-logarithmic of the upconversion emission intensity *versus* the pump power density of the $Ba(Gd_{0.2}Y_{0.8})_{0.78}F_5$ nanocrystals doped with 20 mol% $Yb^{3+}$ and 2 mol% $Tm^{3+}$.

Fig. 10 The mechanism of optical thermal sensing through $Tm^{3+}$ upconversion under infrared excitation and $Gd^{3+}$-$Yb^{3+}$-$Tm^{3+}$ energy transfer in $Ba(Gd_{1-x}Y_x)_{0.78}F_5$: $Yb^{3+}$, $Tm^{3+}$ nanocrystals under infrared excitation.

Fig. 11 CIE chromaticity diagram of the selected $Ba(Gd_{0.2}Y_{0.8})_{0.78}F_5$: $Yb^{3+}$, $Tm^{3+}$ under 980 nm excitation.

Fig. 12 Magnetization-applied magnetic field curves of $Ba(Gd_{1-x}Y_x)_{0.78}F_5$: $Yb^{3+}$, $Tm^{3+}$ ($0 \leq x \leq 0.9$).

**Table. 1** Overview of the hydrothermal conditions of controllable synthesis of the $Ba(Gd_{1-x}Y_x)_{0.78}F_5$: $Yb^{3+}$, $Tm^{3+}$ solid solution nanocrystals.

| Samples $Ba(Gd_{1-x}Y_x)_{0.78}F_5$: Yb, Tm | $Ba(NO_3)_2$ (mL) | $Gd(NO_3)_3$ (mL) | $Y(NO_3)_3$ (mL) | $Yb(NO_3)_3$ (mL) | $Tm(NO_3)_3$ (mL) | $NH_4F$ (mL) |
|---|---|---|---|---|---|---|
| x=0 | 12.50 | 19.50 | 0 | 5.00 | 1.00 | 12.50 |
| x=0.1 | 12.50 | 17.55 | 1.95 | 5.00 | 1.00 | 12.50 |
| x=0.2 | 12.50 | 15.60 | 3.90 | 5.00 | 1.00 | 12.50 |
| x=0.3 | 12.50 | 13.65 | 5.85 | 5.00 | 1.00 | 12.50 |
| x=0.4 | 12.50 | 11.70 | 7.80 | 5.00 | 1.00 | 12.50 |
| x=0.5 | 12.50 | 9.75 | 9.75 | 5.00 | 1.00 | 12.50 |
| x=0.6 | 12.50 | 7.80 | 11.70 | 5.00 | 1.00 | 12.50 |
| x=0.7 | 12.50 | 5.85 | 13.65 | 5.00 | 1.00 | 12.50 |
| x=0.8 | 12.50 | 3.90 | 15.60 | 5.00 | 1.00 | 12.50 |
| x=0.9 | 12.50 | 1.95 | 17.55 | 5.00 | 1.00 | 12.50 |
| x=1.0 | 12.50 | 0 | 19.50 | 5.00 | 1.00 | 12.50 |

**Table 2** Rietveld refinement patterns of the $Ba(Gd_{1-x}Y_x)_{0.78}F_5$: $Yb^{3+}$, $Tm^{3+}$ solid solution nanocrystals.

| **Samples** | **Refined factor** | | | **Lattice parameters** | | | | **Space group** |
|---|---|---|---|---|---|---|---|---|
| | $\chi^2$ | $R_p$(%) | $R_{wp}$(%) | *a* (Å) | *b* (Å) | *c* (Å) | *V* (Å$^3$) | |
| x=0 | 4.606 | 5.53 | 7.59 | 5.900 | 5.900 | 5.900 | 205.379 | *Fm*-3*m* |
| x=0.1 | 1.381 | 3.27 | 4.23 | 5.890 | 5.890 | 5.890 | 204.336 | *Fm*-3*m* |
| x=0.2 | 1.324 | 3.35 | 4.25 | 5.889 | 5.889 | 5.889 | 204.232 | *Fm*-3*m* |
| x=0.3 | 1.079 | 3.07 | 4.01 | 5.885 | 5.885 | 5.885 | 203.817 | *Fm*-3*m* |
| x=0.4 | 1.927 | 4.34 | 5.35 | 5.882 | 5.882 | 5.882 | 203.532 | *Fm*-3*m* |
| x=0.5 | 1.187 | 3.40 | 4.35 | 5.878 | 5.878 | 5.878 | 203.090 | *Fm*-3*m* |
| x=0.6 | 1.991 | 4.34 | 5.67 | 5.877 | 5.877 | 5.877 | 202.986 | *Fm*-3*m* |
| x=0.7 | 2.219 | 4.86 | 6.04 | 5.873 | 5.873 | 5.873 | 202.635 | *Fm*-3*m* |
| x=0.8 | 3.349 | 5.58 | 7.74 | 5.871 | 5.871 | 5.871 | 202.340 | *Fm*-3*m* |
| x=0.9 | 1.078 | 3.53 | 4.42 | 5.870 | 5.870 | 5.870 | 202.246 | *Fm*-3*m* |
| x=1.0 | 2.419 | 5.17 | 6.72 | 5.866 | 5.866 | 5.866 | 201.838 | *Fm*-3*m* |

**Table 3** Atomic percentage of the synthesized $Ba(Gd_{1-x}Y_x)_{0.78}F_5$: $Yb^{3+}$, $Tm^{3+}$ solid solution nanocrystals.

| **Samples** | **Atomic percentage (%)** | | | | | |
|---|---|---|---|---|---|---|
| $Ba(Gd_{1-x}Y_x)_{0.78}F_5$: Yb, Tm | Ba | Gd | Y | Yb | Tm | F |
| x=0 | 17.19 | 14.90 | 0 | 3.87 | 0.60 | 63.43 |
| x=0.1 | 17.03 | 12.81 | 1.27 | 3.78 | 0.42 | 64.69 |
| x=0.2 | 16.10 | 10.51 | 2.48 | 3.53 | 0.50 | 66.88 |
| x=0.3 | 16.57 | 9.65 | 3.91 | 3.56 | 0.48 | 65.84 |
| x=0.4 | 16.44 | 8.12 | 5.33 | 3.52 | 0.38 | 66.22 |
| x=0.5 | 16.20 | 6.78 | 6.57 | 3.31 | 0.40 | 66.74 |
| x=0.6 | 16.95 | 5.70 | 8.34 | 3.56 | 0.39 | 65.05 |
| x=0.7 | 16.49 | 4.33 | 9.72 | 3.56 | 0.36 | 65.54 |
| x=0.8 | 16.34 | 2.72 | 11.04 | 3.36 | 0.35 | 66.20 |
| x=0.9 | 16.78 | 1.32 | 11.90 | 3.67 | 0.39 | 65.95 |
| x=1.0 | 16.76 | 0 | 13.96 | 3.79 | 0.45 | 65.04 |

**Fig. 1**

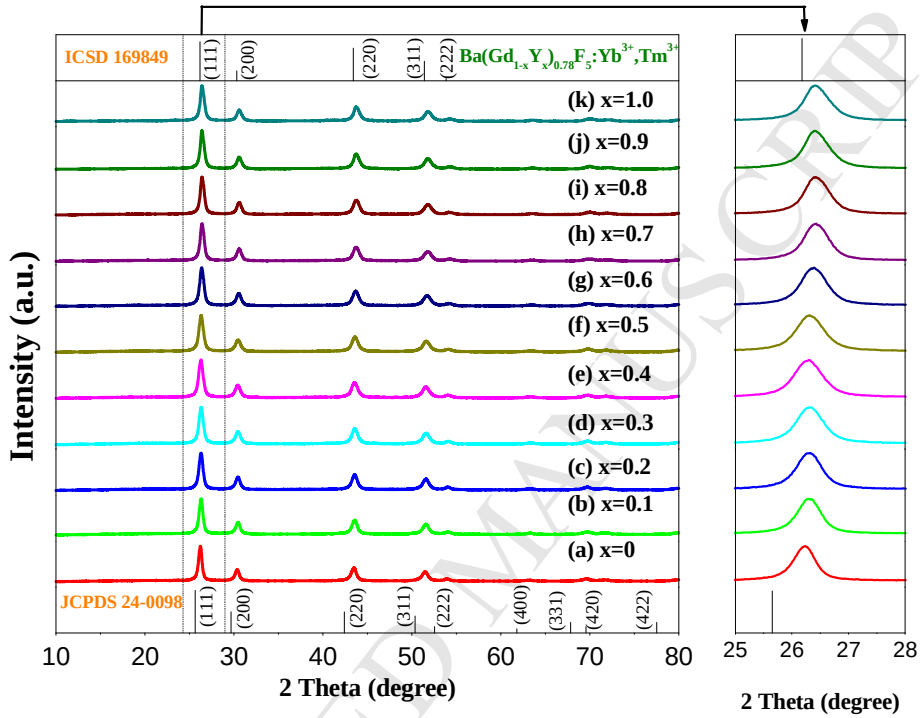

**Fig. 2**

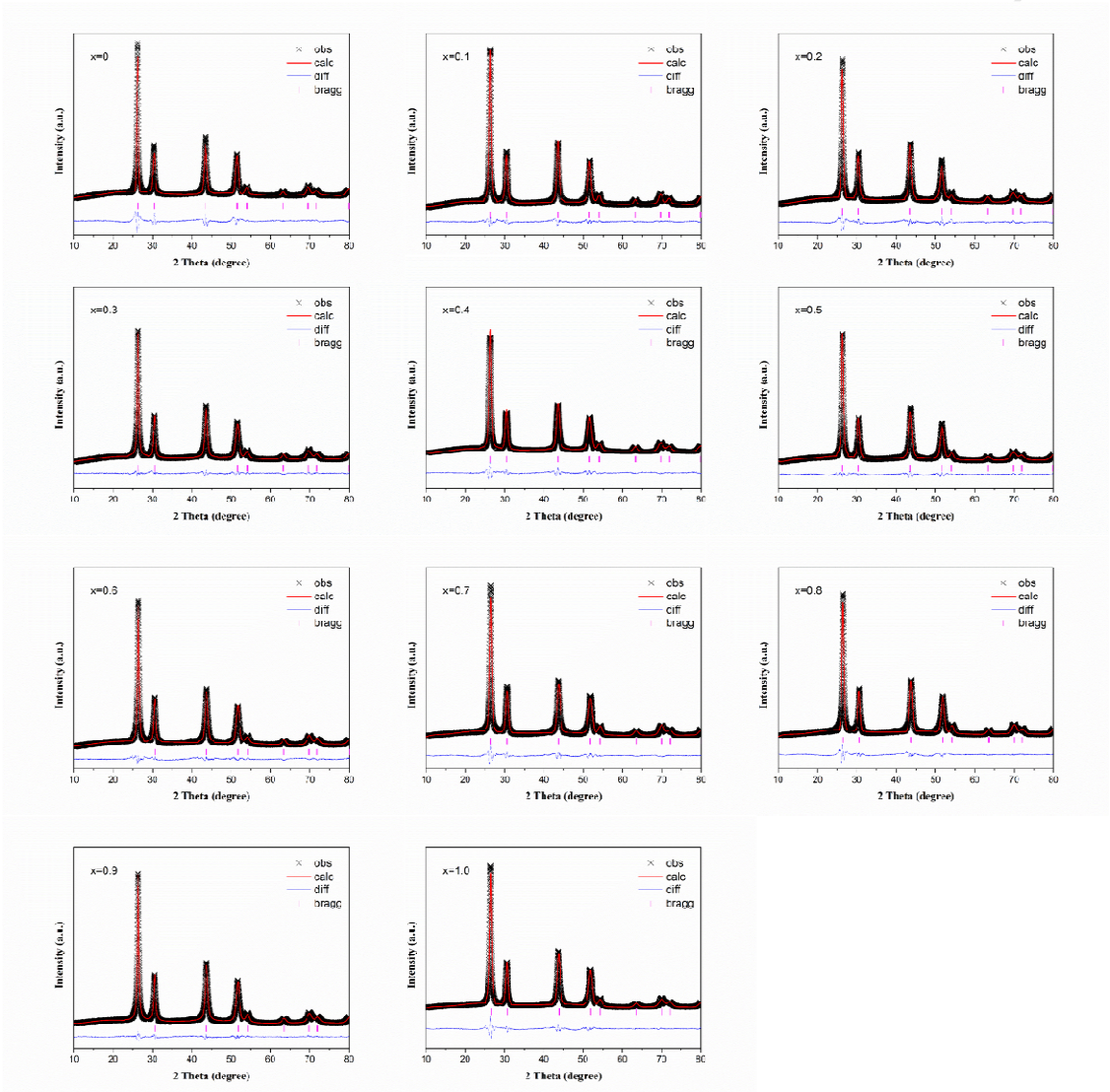
x=0
x=0.1
x=0.2
x=0.3
x=0.4
x=0.5
x=0.6
x=0.7
x=0.8
x=0.9
x=1.0
obs
calc
diff
bragg
Intensity (a.u.)
2 Theta (degree)

**Fig. 3**

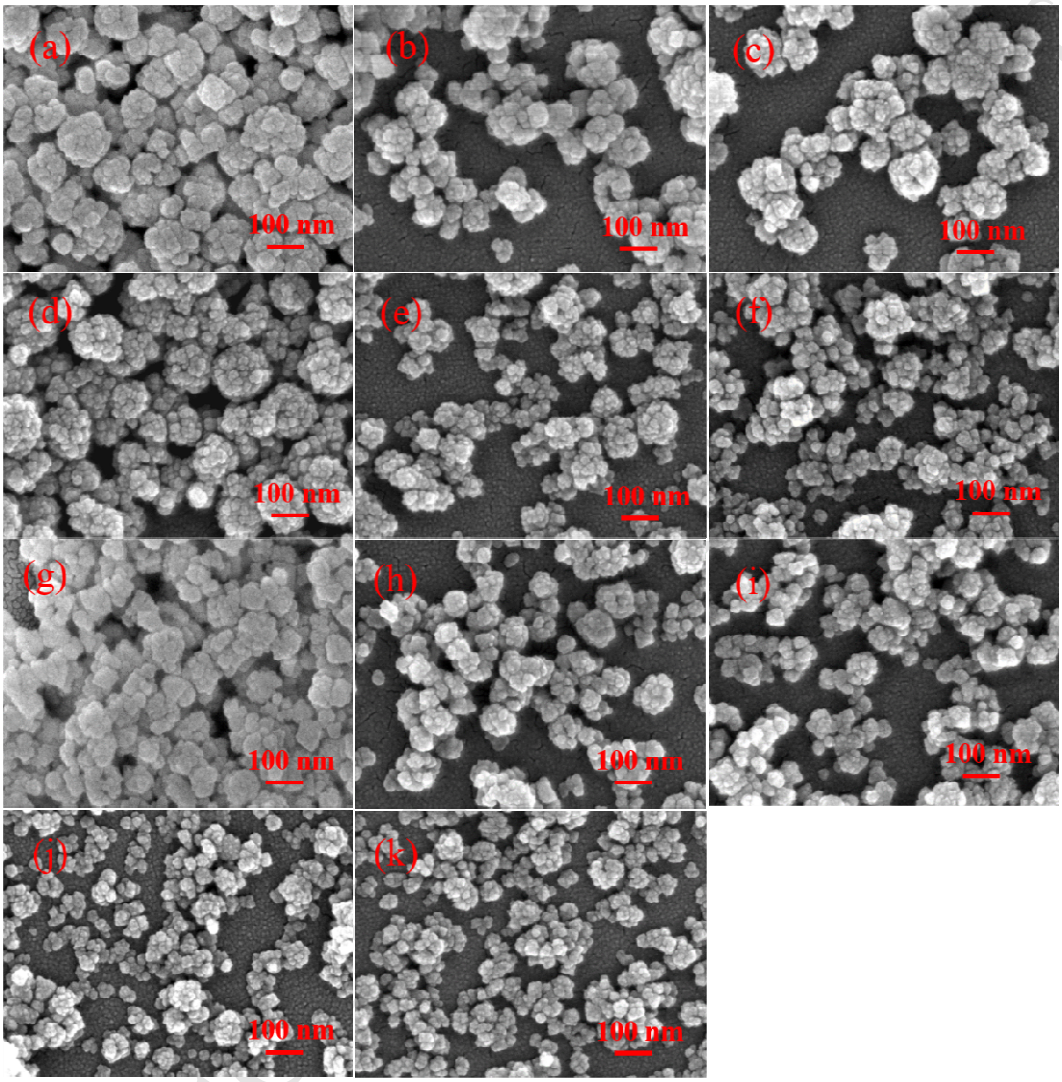
(a)
100 nm
(b)
100 nm
(c)
100 nm
(d)
100 nm
(e)
100 nm
(f)
100 nm
(g)
100 nm
(h)
100 nm
(i)
100 nm
(j)
100 nm
(k)
100 nm

**Fig. 4**

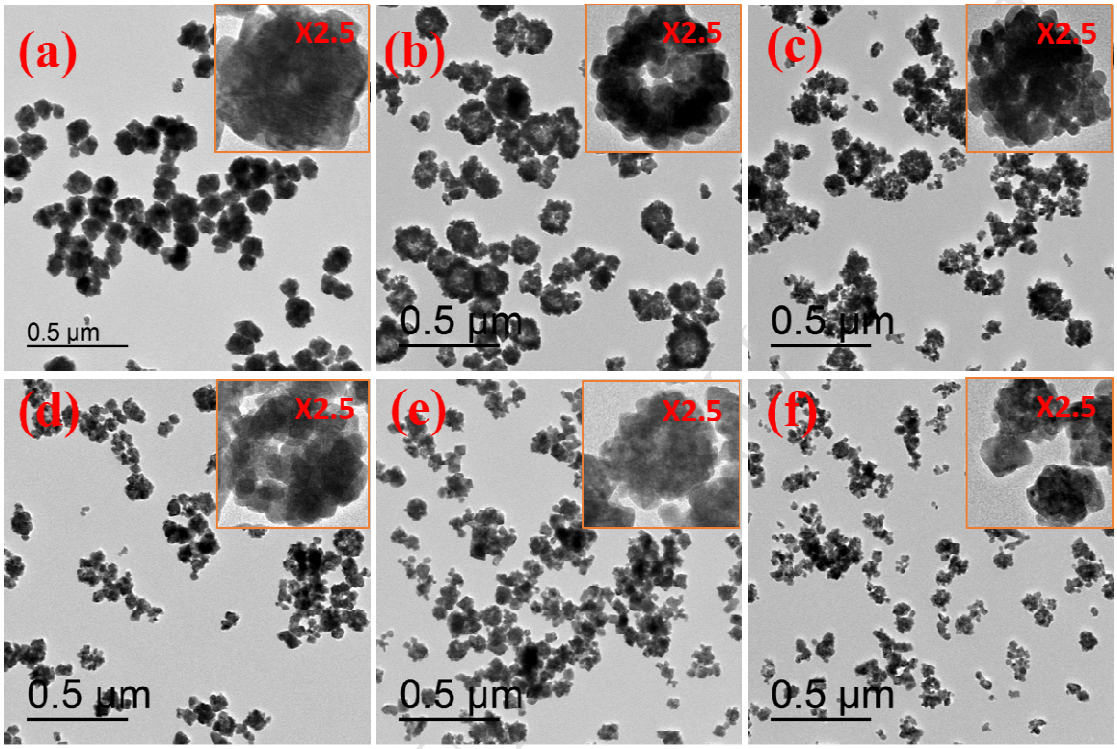

**Fig. 5**

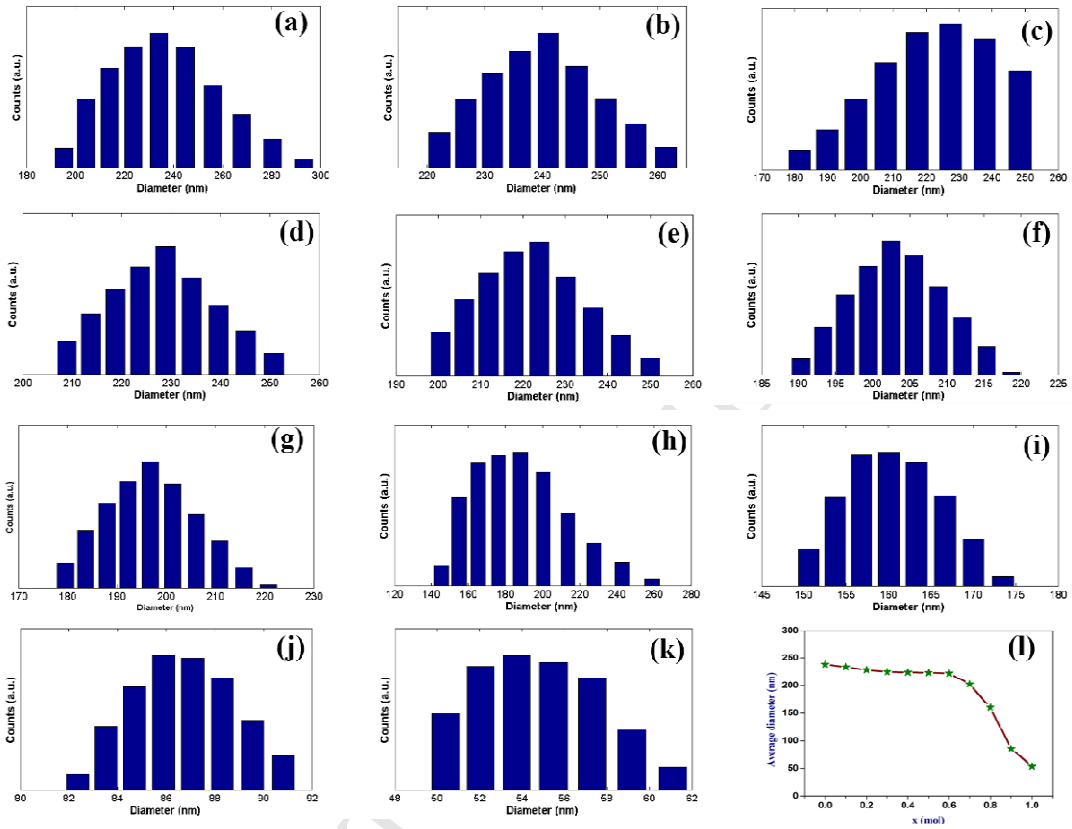

**Fig. 6**

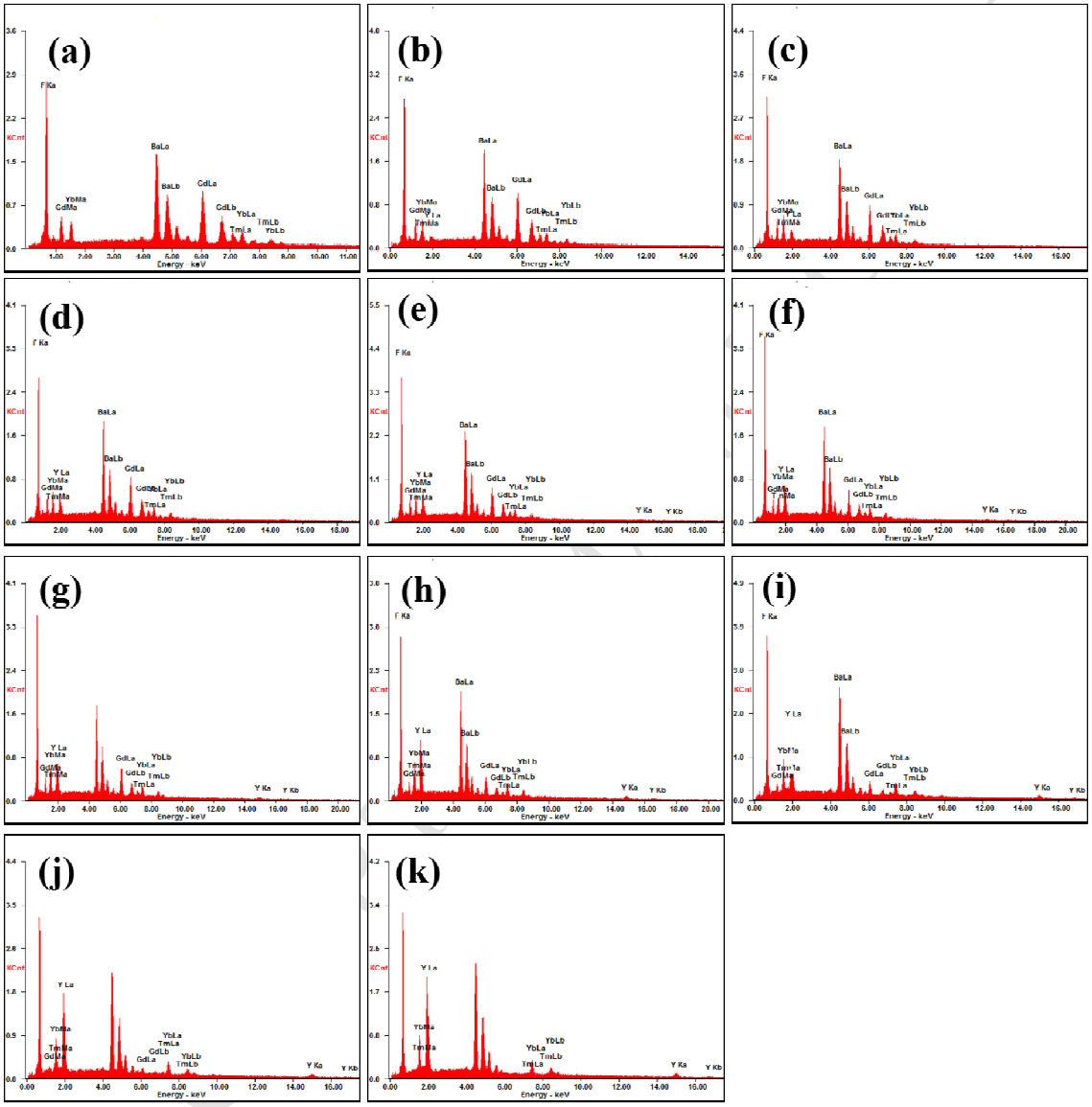

**Fig .7**

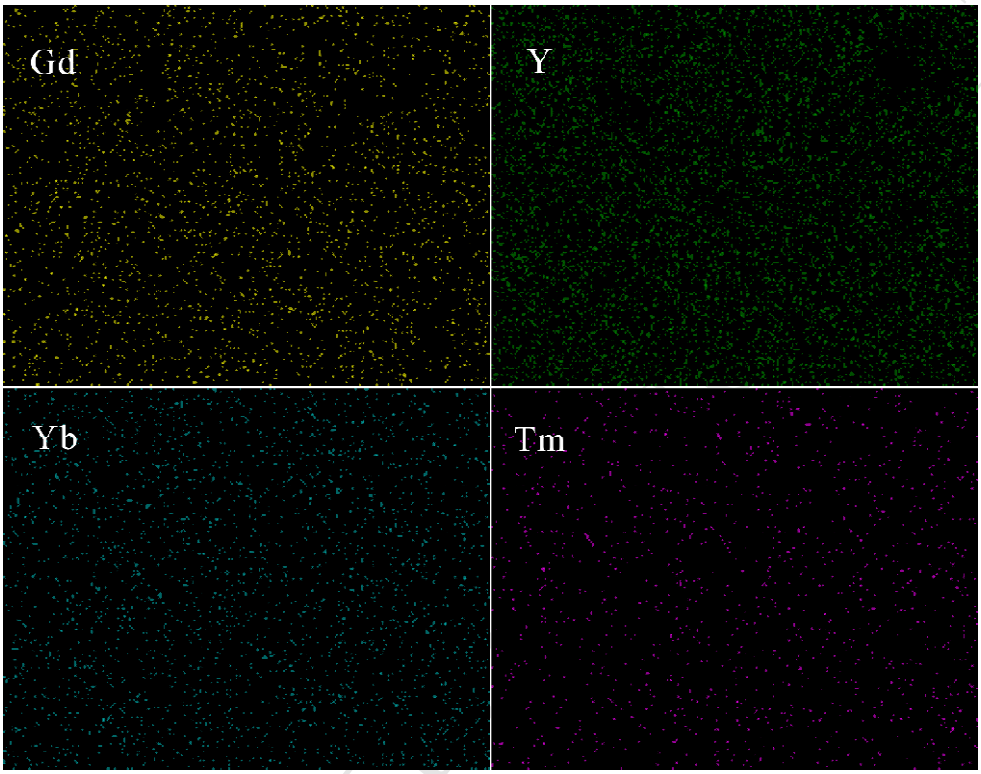

**Fig. 8**

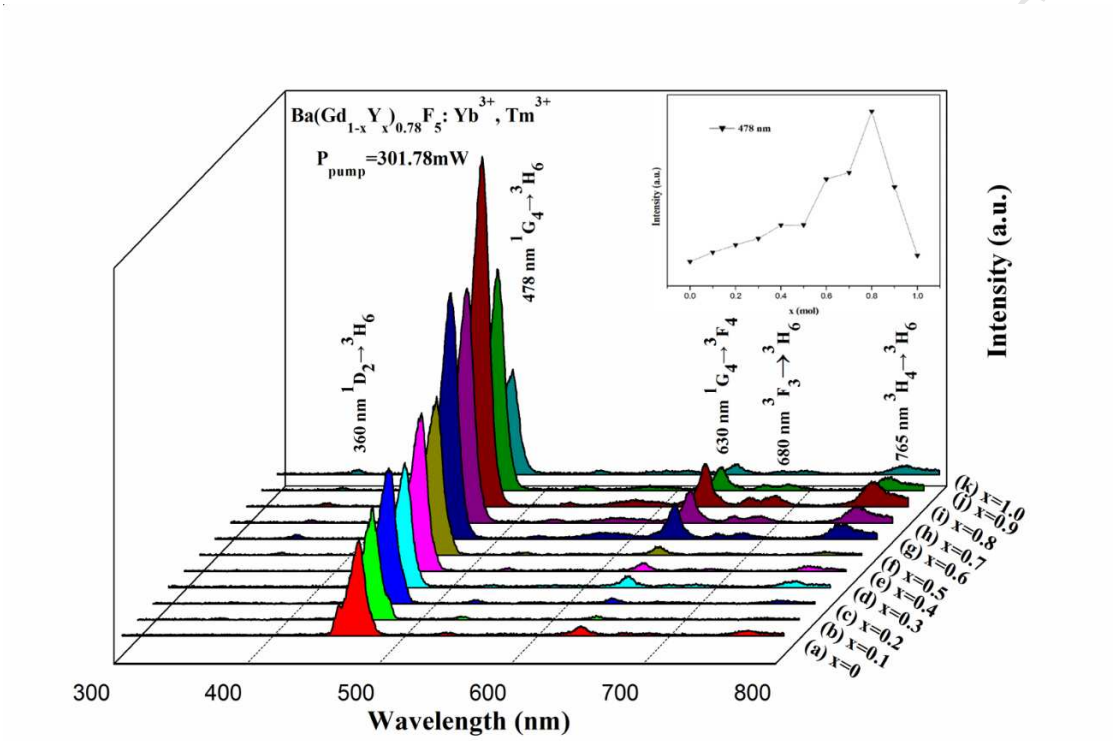

**Fig. 9**

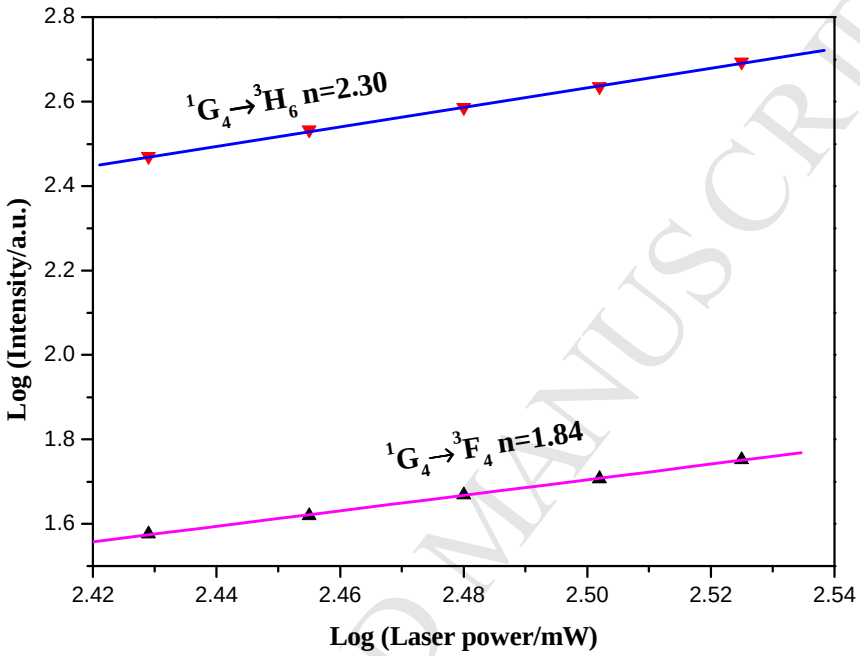

**Fig. 10**

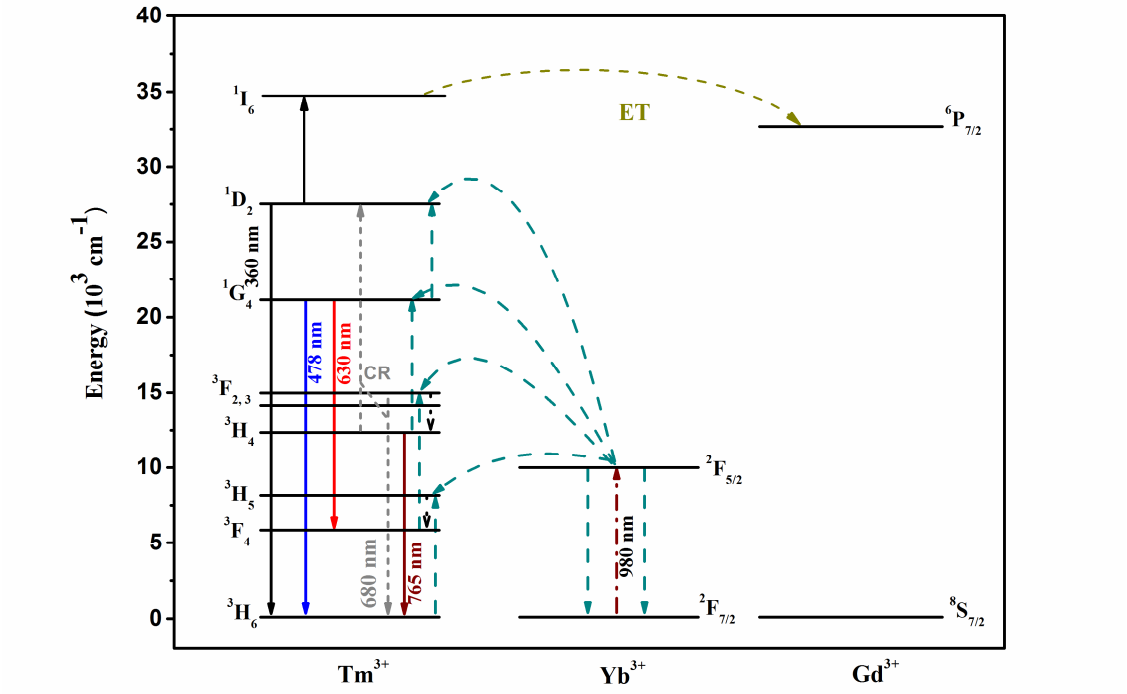
Energy ($10^3$ cm$^{-1}$)
40
35
30
25
20
15
10
5
0
$^1I_6$
$^1D_2$
$^1G_4$
$^3F_{2,3}$
$^3H_4$
$^3H_5$
$^3F_4$
$^3H_6$
$^6P_{7/2}$
$^2F_{5/2}$
$^2F_{7/2}$
$^8S_{7/2}$
ET
360 nm
478 nm
630 nm
CR
680 nm
765 nm
980 nm
$Tm^{3+}$
$Yb^{3+}$
$Gd^{3+}$

**Fig. 11**

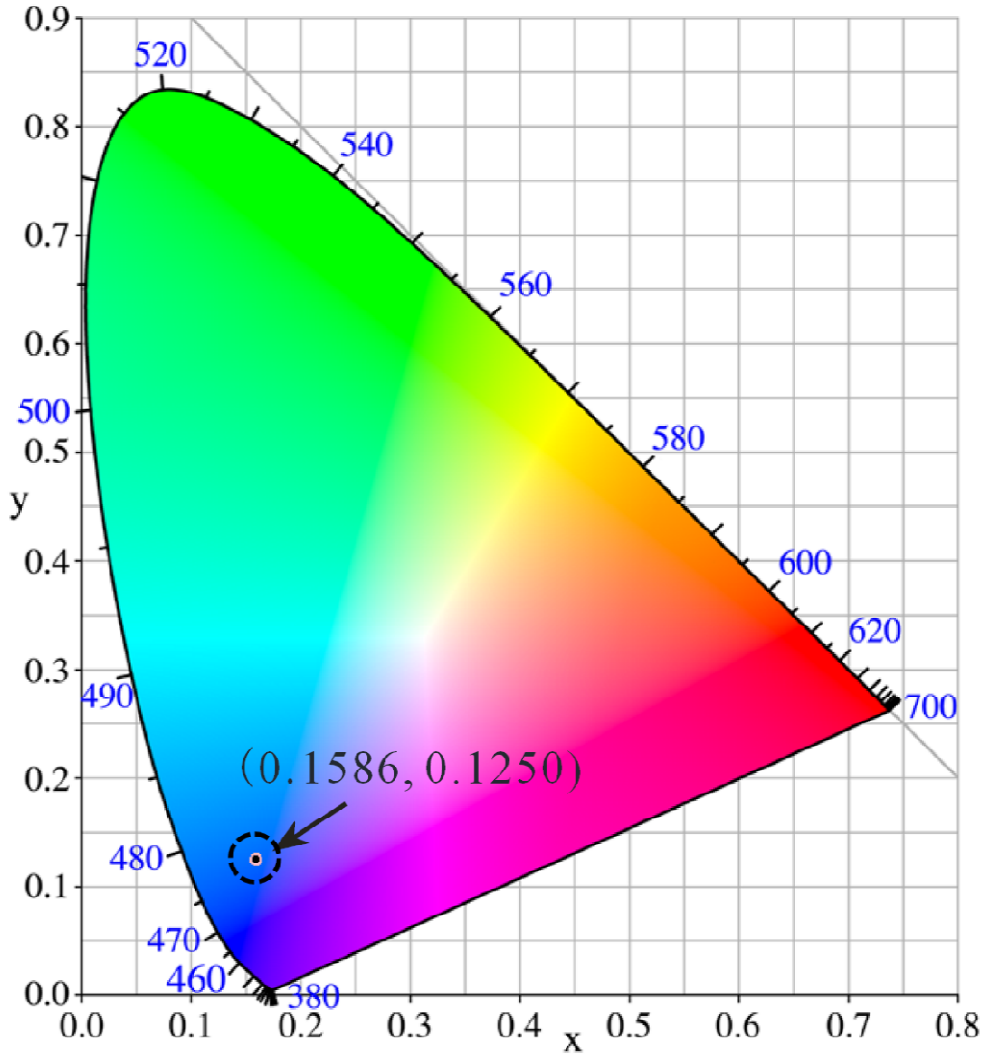
0.9
0.8
0.7
0.6
500
0.5
y
0.4
0.3
490
0.2
480
0.1
470
460
0.0
520
540
560
580
600
620
700
380
(0.1586, 0.1250)
0.0
0.1
0.2
0.3
0.4
x
0.5
0.6
0.7
0.8

**Fig. 12**

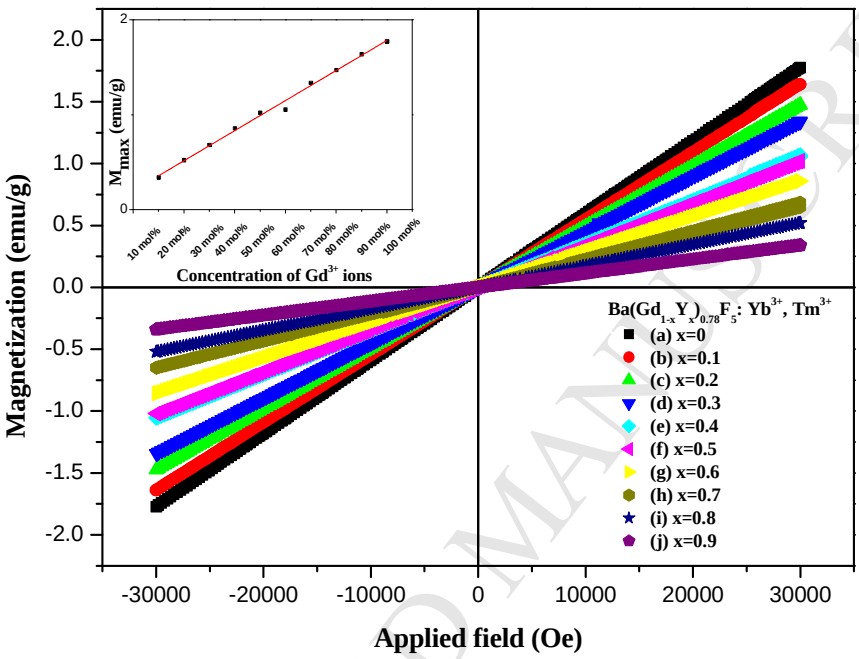

# Highlights

1. Novel $Ba(Gd_{1-x}Y_x)_{0.78}F_5:Yb^{3+},Tm^{3+}$ nanocrystals have been proposed and synthesized.

2. The UC enhancement mechanism of the co-doped nanocrystals have been proposed.

3. This work may provide a guidance to design for other fluoride solid solution systems.